

Understanding Corrosion Inhibition of iron by 2-Thiophenecarboxylic Acid Methyl Ester: Electrochemical and Computational study

K.F.Khaled^{1,2,*}, N. S. Abdel-Shafi² and N. A. Al-Mobarak³

¹ Materials and Corrosion Lab., Chemistry Department, Faculty of Science. Taif University, Taif, Kingdom of Saudi Arabia

² Electrochemistry Research Lab., Chemistry Department, Faculty of Education. Ain Shams University, Roxy, Cairo, Egypt

³ Chemistry Department, Faculty of Science, Princess Nora bint Abdulrahman University, Riyadh, Saudi Arabia

*E-mail: khaledrice2003@yahoo.com

Received: 10 July 2011 / Accepted: 3 January 2012 / Published: 1 February 2012

The inhibiting effect of 2-thiophenecarboxylic acid methyl ester, TME on iron corrosion in 1.0 M HCl solutions were evaluated using several electrochemical measurements includes potentiodynamic polarization, electrochemical impedance spectroscopy and electrochemical frequency modulation techniques. Adsorption mechanism of TME on iron surface was explored by explicit solvent simulations using molecular dynamics and quantum chemical calculations. Molecular dynamics simulation techniques are used to calculate the adsorption energy as well as the binding energy between the TME molecule and the iron surface. Also, Adsorption density of the inhibitor molecules on iron surface was calculated using Metropolis Monte Carlo method. Experimental investigations of the studied thiophene derivative show that it reduces the corrosion rate of iron remarkably as its concentration increases. Polarization studies show that TME molecules act as cathodic-type inhibitor. The presence of sulphur and oxygen atoms as well as π -electrons enables the interaction and bonding between TME and the iron surface.

Keywords: Corrosion; Iron; EFM; Molecular dynamics; Quantum chemical calculations

1. INTRODUCTION

The corrosion of iron and steel are the most common form of corrosion, especially in acid solution. It has practical importance, for example, in the acid pickling of iron and steel, chemical cleaning of the scale in metallurgy, oil recovery and petrochemical industry, and other electrochemical

systems [1]. The use of inhibitors is one of the most practical methods for protection against corrosion in acidic media [2]. Some organic compounds are found to be effective corrosion inhibitors for many metals and alloys. It has been commonly recognized that organic inhibitor usually promotes formation of a chelate on the metal surface, which includes the transfer of electrons from the organic compounds to metal, forming coordinate covalent bond during such chemical adsorption process [3]. In this way, the metal acts as an electrophile, whereas the nucleophile centers of inhibitor molecule are normally hetero atoms with free electron pairs which are readily available for sharing, to form a bond. The most common organic substances with these characteristics are those containing O, N and/or S atoms [4]. Among the various organic inhibitors used for inhibiting the corrosion of iron and steel in acid medium, thiophene derivatives that proved very good for inhibition of metal corrosion in acidic solutions [5-9].

In this paper we report on the use of 2-thiophenecarboxylic acid methyl ester, TME as possible corrosion inhibitor for iron in 1.0 M HCl using several electrochemical methods. One of the most recent electrochemical techniques which will be used in this study is electrochemical frequency modulation, EFM which is used as a powerful tool for corrosion rate measurements [10-12]. EFM yields a remarkable amount of information on the corrosion process including corrosion rate, Tafel constants and causality factors. The corrosion rate is calculated from the corrosion current density that is measured by EFM [13]. It is important to emphasize that Tafel constants are not needed to calculate the corrosion current density in EFM. Because of that, EFM enjoys a significant practical advantage compared to polarization techniques. EFM can be used as a rapid and non-destructive technique for corrosion rate measurements without prior knowledge of Tafel constants.

Many computational approaches exist for understanding the adsorption of the inhibitor molecules on the metal surface. These typically use quantum chemical calculation and molecular dynamics simulations to understand the inhibition mechanism of inhibitors on the metal surface [14,15].

The present work describes the use of 2-thiophenecarboxylic acid methyl ester TME, as possible inhibitor, for the corrosion of iron in 1.0 M HCl solution. Measurements were conducted based on electrochemical measurements include, potentiodynamic polarization, impedance and EFM techniques. To explore the adsorption mechanism of TME on iron surface, explicit solvent simulations using molecular dynamics and quantum chemical calculation will be used to study the adsorption of TME on iron surface. It is also the aim of this work to study the adsorption of TME using molecular dynamics simulation techniques to calculate the adsorption energy as well as the binding energy between the inhibitor molecule and the iron surface. Also, Adsorption density of the inhibitor molecules on iron surface will be calculated using Metropolis Monte Carlo method.

2. EXPERIMENTAL DETAILS

All solutions were freshly prepared from analytical grade chemical reagents using doubly distilled water and were used without further purification. For each run, a freshly prepared solution was used.

Electrochemical corrosion tests have been carried out on electrodes cut from iron (Puratronic 99.99%, CAS 7439-89-6) from Johnson Matthey Ltd. Iron rods were mounted in Teflon (surface area 0.28 cm²). The surface preparation of the specimens was carried out using emery papers of different grads up to 4/0 grit size, rinsed with double distilled water, degreased with acetone and dried at room temperature before use. Hydrochloric acid solutions were prepared from concentrated acid and double distilled water. All experiments were conducted at 30 °C.

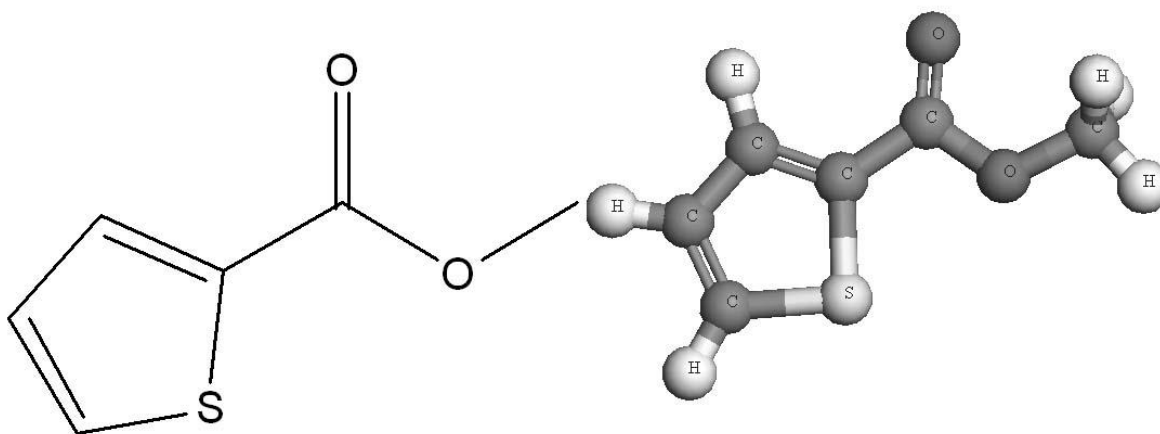


Figure 1. The molecular structure of the investigated 2-thiophenecarboxylic acid methyl ester

The solutions were prepared by mixing hydrochloric acid (Fisher Scientific) with the inhibitor obtained from (Sigma-Aldrich Chemical Co.), which used without any pre-treatment. Fig. 1 shows the molecular structure of the investigated 2-thiophenecarboxylic acid methyl ester, TME. The electrochemical cell used has described elsewhere [16]. The reference electrode was a saturated calomel electrode (SCE). All reported potential values are referred to this type of electrode. Polarization and impedance measurements were carried out under static conditions at 30 °C with a fine Luggin capillary to avoid ohmic resistance.

Measurements were performed on EG&G Princeton Applied Research potentiostat/galvanostat (PAR model 273) in combination with a Solarton 1250 frequency response analyzer. These were used for polarization and capacitance measurements along with a computer for collecting data. The potentiodynamic current/potential curves were obtained by changing the electrode potential automatically from -750 to -300 mV_{SCE} with scan rate of 5 mV s⁻¹. EIS measurements were carried out in frequency range of 100 kHz to 30 mHz with amplitude of 5 mV peak-to-peak using a.c. signals at open circuit potential. The software used in this study is corrosion software, model 352-252 version 2.23, EIS software model 398, ZsimDemo v 3.22 for equivalent circuit analysis and Sigma Plot v. 11.0 for graphing data.

Electrochemical Frequency Modulation (EFM) is used to calculate the corrosion current density in absence and presence of different concentrations of TME. In this study, we use a perturbation signal with amplitude of 10mV for both perturbation frequencies of 2 and 5 Hz. The choice for the frequencies of 2 and 5 Hz was based on three opinions [11]. First, the harmonics and

intermodulation frequencies should not manipulate each other. Second, the frequency should be as low as possible to avoid influence of the capacitive behavior of the electrochemical double layer. Third, the frequency should be as large as possible to reduce time needed to perform a measurement.

EFM measurements were performed with a Gamry Instrument Potentiostat/Galvanostat/ZRA. These include Gamry framework system based on the ESA400, Gamry applications that include EFM140© software. Echem Analyst 5.58 software was used for plotting, graphing and fitting data.

3. THEORETICAL CALCULATIONS

3.1 Quantum chemical calculations

Density functional theory (DFT) has been widely used for analysis of inhibitor efficiency and inhibitor-surface interaction. In this study, the geometric configuration of a molecule involved was optimized with DFT/B3LYP method with basis set of 6-31G*. A full optimization of all geometrical variables without any symmetry constraint was performed. DFT develops the molecular orbitals on a valence basis set and also calculates electronic properties and the optimized geometries of the thiophene derivative molecule, TME.

Atomic Fukui indices, which are obtained from the electron density, is useful in predicting which atoms in a molecule are most likely to suffer nucleophilic, electrophilic or radical attacks. The reactivity of the TME was analyzed through an evaluation of the Fukui indices [17], which is a measurement of the chemical reactivity, as well as an indicative of the reactive regions and the nucleophilic and electrophilic behaviour of the inhibitor molecule.

The regions of a molecule where the Fukui function is large are chemically softer than the regions where the Fukui function is small, and by invoking the HSAB principle in a local sense, one may establish the behaviour of the different sites with respect to hard or soft reagents [15].

The Fukui function $f(\vec{r})$ is defined as the first derivative of the electronic density $\rho(\vec{r})$ with respect to the number of electrons N at a constant external potential $v(\vec{r})$

$$f(\vec{r}) = \left(\frac{\partial \rho(\vec{r})}{\partial N} \right)_{v(\vec{r})} \quad (1)$$

If the effects of relaxation associated with the addition or removal of electronic charges are not considered, then

$$\rho^+(\vec{r}) \approx \rho_{LUMO}(\vec{r}) \quad (2)$$

$$\rho^-(\vec{r}) \approx \rho_{HOMO}(\vec{r}) \quad (3)$$

where $\rho_{LUMO}(\vec{r})$ is the density of the lowest unoccupied molecular orbital and $\rho_{HOMO}(\vec{r})$ is density of the highest occupied molecular orbital [18].

The condensed Fukui functions [17] are calculated by taking the finite difference approximations from Mulliken population analysis of atoms in TME molecule, depending on the direction of the electron transfer

$$f_k^+ = q_k(N+1) - q_k(N) \text{ (for nucleophilic attack)} \quad (4)$$

$$f_k^- = q_k(N) - q_k(N-1) \text{ (for electrophilic attack)} \quad (5)$$

$$f_k^o = \frac{q_k(N+1) - q_k(N-1)}{2} \text{ (for radial attack)} \quad (6)$$

where q_k is the gross charge of atom k in the molecule i.e. the electron density at a point r in space around the molecule. The N corresponds to the number of electrons in the molecule. $N+1$ corresponds to an anion, with an electron added to the LUMO of the neutral molecule. $N-1$ correspondingly is the cation with an electron removed from the HOMO of the neutral. All calculations are done at the ground-state geometry. These functions can be condensed to the nuclei by using an atomic charge partitioning scheme, such as Mulliken population analysis in equations 4-6.

3.2 Molecular dynamics simulation

The molecular dynamics MD simulation of the interaction between thiophene derivative, TME and Fe (110) surface was carried out in a simulation box ($7.44 \text{ \AA} \times 7.44 \text{ \AA} \times 25.13 \text{ \AA}$) with periodic boundary conditions to model a representative part of the interface devoid of any arbitrary boundary effects. The Fe (110) surface was first built and relaxed by minimizing its energy using molecular mechanics, then the surface area of Fe (110) was increased and its periodicity is changed by constructing a super cell, and then a vacuum slab with 15 \AA thicknesses was built on the Fe (110) surface. The number of layers in the structure was chosen so that the depth of the surface is greater than the non-bond cutoff used in calculation. Using 6 layers of iron atoms gives a sufficient depth that the TME molecules will only be involved in non-bond interactions with iron atoms in the layers of the surface, without increasing the calculation time unreasonably [19]. This structure then converted to have 3D periodicity. As 3D periodic boundary conditions are used, it is important that the size of the vacuum slab is great enough (15 \AA) that the non-bond calculations for the adsorbate does not interact with the periodic image of the bottom layer of atoms in the surface. After minimizing the Fe (110) surface and TME molecules, the corrosion system will be built by layer builder to place the TME molecules on Fe (110) surface, and the adsorption of these molecules on the Fe (110) surface were simulated using the COMPASS (condensed phase optimized molecular potentials for atomistic simulation studies) force field. The adsorption of TME molecule onto Fe (110) surface provides access to the energetic of the adsorption and its effects on the inhibition efficiencies of TME molecules [19].

The binding energy between TME molecules and Fe (110) surface were calculated using equation 7 [20]:

$$E_{\text{binding}} = E_{\text{total}} - (E_{\text{surface}} + E_{\text{inhibitor}}) \quad (7)$$

Where E_{total} is the total energy of the surface and inhibitor, E_{surface} is the energy of the surface without the inhibitor, and $E_{\text{inhibitor}}$ is the energy of the inhibitor without the surface.

Fukui indices, quantum chemical parameters, adsorption and binding energies are calculated by using Materials Studio DMol³ and Adsorption locator version 5.0 [21,22], a high quality quantum mechanics computer program (available from Accelrys, San Diego, CA). These calculations employed an ab initio, local density functional (LDF) method with a double numeric polarization (DNP) basis set and a Becke-Perdew (BP) functional. Dmol³ use a Mulliken population analysis [23].

4. RESULTS AND DISCUSSION

4.1 Electrochemical measurements

4.1.1 EFM measurements

Electrochemical frequency modulation, EFM is a technique for corrosion rate measurements. Results obtained with the EFM technique were shown in Fig. 2.

Each plot in Fig. 2 is a spectrum, (an intermodulation spectrum). The two large peaks, in Fig. 2 are the response to the 2 and 5 Hz excitation frequencies. The peaks in Fig. 2 are the harmonics, sums, and differences of the two excitation frequencies. These peaks are used by the EFM140 software package to calculate the corrosion current and Tafel constants. There is nearly no response (<100 nA) at 4.5 Hz, for example; the frequencies and amplitudes of the peaks are not coincident.

Corrosion kinetic parameters listed in Table 1 are calculated from EFM technique, using Eqs. 8-12 [11]:

$$i_{\text{corr}} = \frac{i_{\omega}^2}{\sqrt{48(2i_{\omega}i_{3\omega} - i_{2\omega}^2)}} \quad (8)$$

$$\beta_a = \frac{i_{\omega}U_o}{2i_{2\omega} + 2\sqrt{3}\sqrt{2i_{3\omega}i_{\omega} - i_{2\omega}^2}} \quad (9)$$

$$\beta_c = \frac{i_{\omega}U_o}{2\sqrt{3}\sqrt{2i_{3\omega}i_{\omega} - i_{2\omega}^2} - 2i_{2\omega}} \quad (10)$$

$$\text{Causality factor (2)} = \frac{i_{\omega_2 \pm \omega_1}}{i_{2\omega_1}} = 2.0 \quad (11)$$

$$\text{Causality factor (3)} = \frac{i_{2\omega_2 \pm \omega_1}}{i_{3\omega_1}} = 3.0 \quad (12)$$

where i is the instantaneous current density at the working electrode measured at frequency ω and U_o is the amplitude of the sine wave distortion.

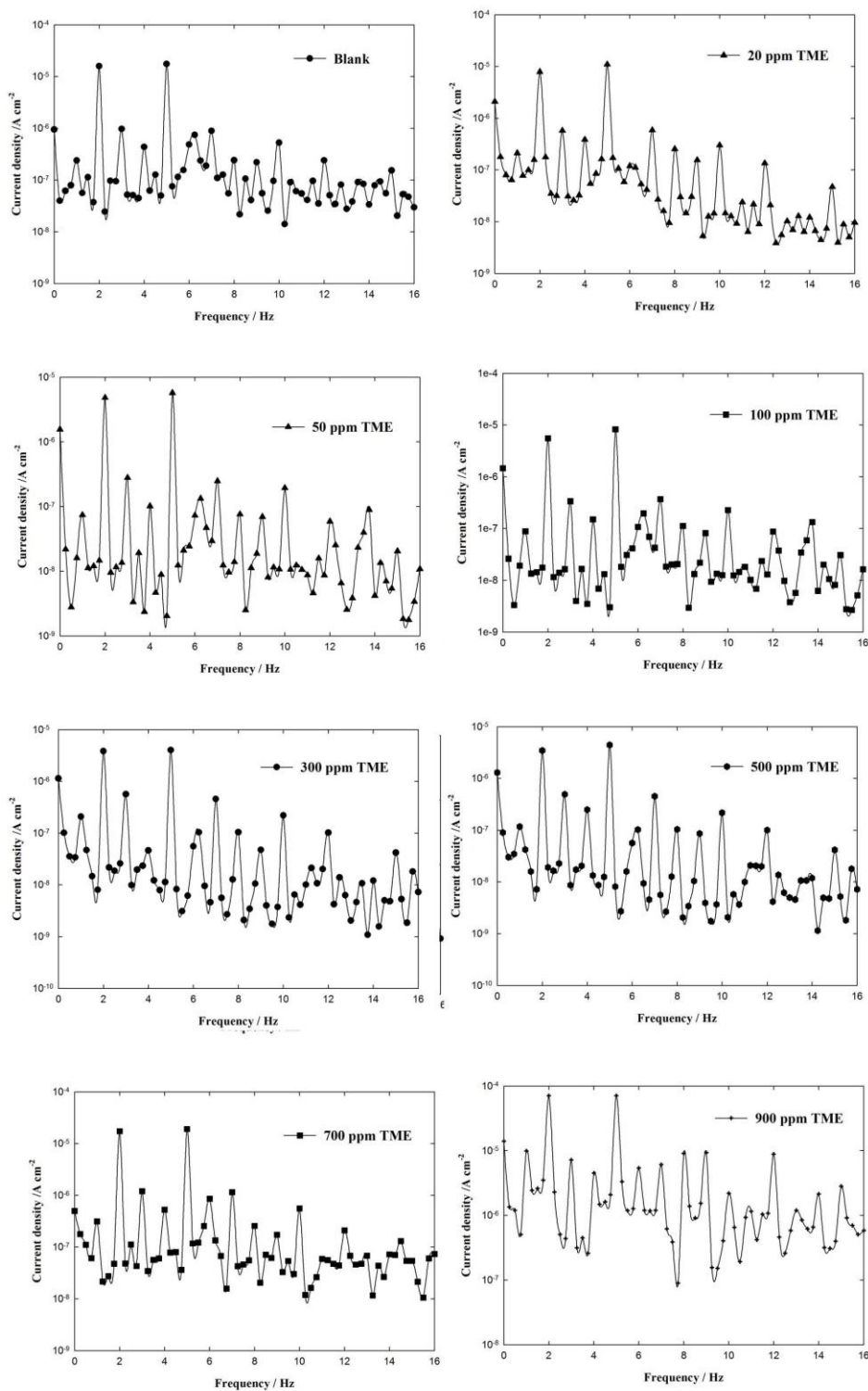


Figure 2. Intermodulation spectrum for iron in 1.0 M HCl in absence and presence of various concentrations of TME in 1.0 M HCl at 30 °C ±1.

Table 1. Electrochemical kinetic parameters obtained by EFM technique for iron in absence and presence of various concentrations of TME in 1.0 M HCl at 30 °C ±1.

[Inhib]	$(i_{corr}) / \mu\text{A cm}^{-2}$	$\beta_a / \text{mV dec}^{-1}$	$\beta_c / \text{mV dec}^{-1}$	C.R. mpy	CF-2	CF-3	$E_{EFM} \%$
Blank	26.02	85.1	120.1	42.44	1.93	2.31	---
20 ppm	14.3	77	115.2	23.32	1.78	2.15	45.04
50 ppm	11.64	90.3	125.0	18.98	1.85	1.39	55.26
100 ppm	9.72	90.1	122.3	15.85	1.87	2.10	62.64
300 ppm	8.32	85.1	114.3	13.56	1.98	2.05	68.02
500 ppm	4.86	83.3	101.2	7.926	2.00	2.45	81.32
700 ppm	3.12	91.2	112.5	5.088	1.99	2.76	88.00
900 ppm	0.78	89.3	102.1	1.272	1.98	2.89	97.00

Table 1 shows the corrosion kinetic parameters such as inhibition efficiency ($E_{EFM} \%$), corrosion current density ($\mu\text{A cm}^{-2}$), Tafel constants (β_a , β_c) and causality factors (CF-2, CF-3) as a function of inhibitor concentration.

As can be seen from Table 1, i_{corr} values decrease, while those of $E_{EFM} \%$ increase with increase in the inhibitor concentration.

$$E_{EFM} \% = \left(1 - \frac{i_{corr}}{i_{corr}^o}\right) \times 100 \quad (13)$$

where i_{corr}^o and i_{corr} are corrosion current densities in the absence and presence of the inhibitor, respectively. The values of the causality factors in Table 1 which are very close to theoretical values according to the EFM theory [12,24] indicate that the measured data are of good quality. The standard values for CF-2 and CF-3 are 2.0 and 3.0, respectively. The causality factors serve as an internal check on the validity of the EFM measurement.

4.1.2 Electrochemical impedance spectroscopy, EIS measurements

The following EIS results can be interpreted in terms of the equivalent circuit of the electrical double layer shown in Fig. 3, which was used previously to model the iron/acid interface [25]. The effects of TME on the impedance behaviour of iron in 1.0 M HCl solutions are given in Fig. 4. Figure 4 shows a typical set of Nyquist plots for iron in 1.0 M HCl in the absence and presence of various concentrations of TME. It is clear from these plots that the impedance response of iron has significantly changed after the addition of TME in the acid solutions. This indicates that the impedance of an inhibited substrate increases with increasing concentration of inhibitor in 1.0 M HCl. It is clear from Fig. 4 that the change in concentration of TME did not alter the profile of the impedance behaviour, suggesting similar mechanism for the corrosion inhibition of iron by TME.

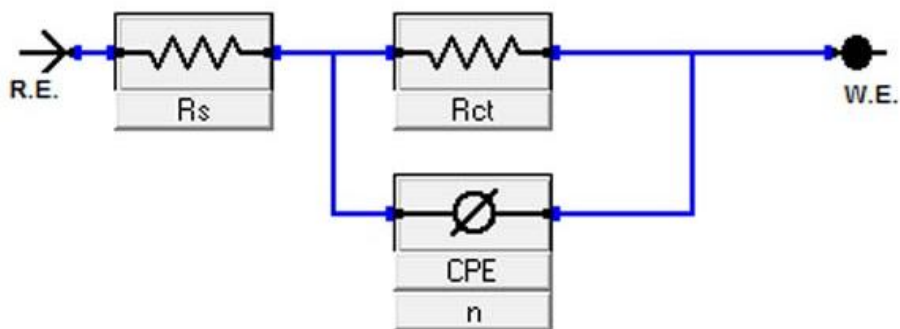


Figure 3. Equivalent circuit used to model impedance data for iron in 1.0 M HCl in absence and presence of various concentrations of TME 30 °C ±1

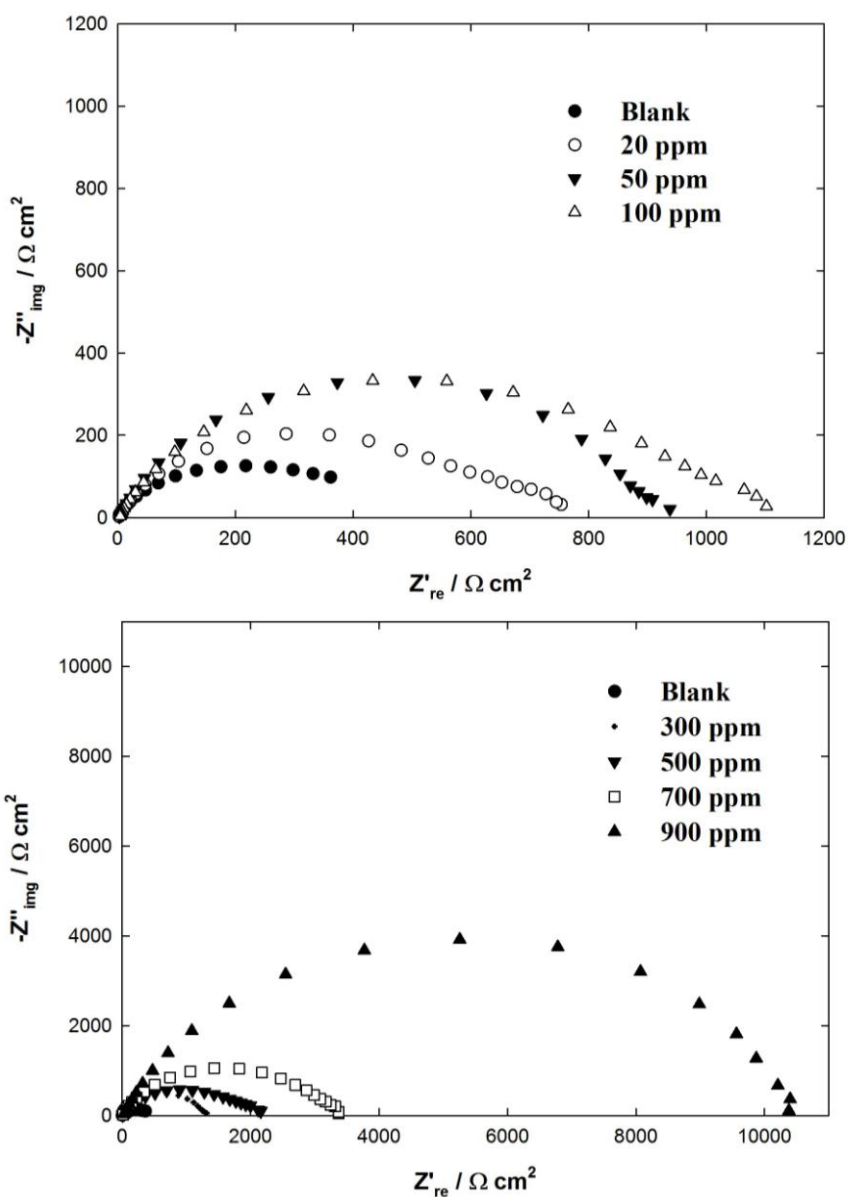


Figure 4. Complex plane impedance plots for iron in 1.0 M HCl in the absence and presence of various concentrations of of TME at 30 °C ±1

As there is a concentration-dependent difference in low frequency region, all experimental spectra had however a form of a depressed semicircle in the Nyquist plots, with the center under real axis.

Table 2. Electrochemical parameters calculated from EIS measurements on iron electrode in 1.0 M HCl solutions without and with various concentrations of TME at 30 ± 1 °C using equivalent circuit presented in Fig. 3.

[Inhib]	$R_s / \Omega \text{ cm}^2$	$R_{ct} / \Omega \text{ cm}^2$	CPE $\mu\Omega^{-1} \text{ cm}^{-2} \text{ S}^n$	n	$\tau_{\text{EIS}} \%$
Blank	0.9	448	210	0.73	---
20 ppm	1.3	772.1	45	0.87	41.9
50 ppm	1.6	945.2	36	0.81	52.6
100 ppm	1.8	1114.9	27	0.76	59.8
300 ppm	1.4	1333.1	18	0.69	66.4
500 ppm	1.8	2221.1	12	0.82	79.8
700 ppm	1.6	3394	10	0.79	86.8
900 ppm	2.4	10420	7	0.91	95.7

Such behaviour is typical for solid metal electrodes and is referred to frequency dispersion of impedance data. Although numerous theoretical elaborations can be found in the literature regarding this subject, a clear and straightforward explanation how this phenomenon relates to metal corrosion remains yet to be seen. However, it has been generally accepted to use one or more so called distributed circuit elements [26] in an equivalent circuit to account for a non-ideal frequency response of solid electrodes. The most widely used is Constant Phase Element (CPE), which has a non-integer power dependence on the frequency ($\omega = 2\pi f$):

$$Y = 1/Z = Y_o (i\omega)^n \quad (14)$$

where Y and Z denote admittance and impedance respectively. Y_o is a frequency independent real constant. The exponent n is fractional [27]. Constant phase element, CPE is believed to be usually attributed to some kind of inhomogeneity of the surface. For $n = 0$, it represents a resistance with $R = Y_o^{-1}$, for $n = 1$ capacitance with $C = Y_o$, for $n = 0.5$ a Warburg and for $n = -1$ an inductance with $L = Y_o^{-1}$ [27,28].

4.1.2.1 Equivalent circuit

All impedance spectra were measured at the respective corrosion potential and are analyzed in terms of the equivalent circuit shown in Fig. 3. Generally this circuit falls into the classic parallel capacitor and resistor combination. ZSimDemo V 3.22 software used for impedance data analysis and the fitting parameters are listed in Table 2, where R_s , R_{ct} , CPE, n are solution resistance, polarization

resistance (charge transfer resistance), constant phase element and exponent term, respectively. The impedance spectra described by semi-circles in the complex plane to first approximation. The semicircle is indicative of a charge transfer process occurring with charge transfer resistance, R_{ct} in parallel with the interfacial capacitance. A large charge transfer resistance is associated with a slowly corroding system. Considering the impedance of a double layer does not behave as an ideal capacitor in the presence of dispersing effect, a constant phase element CPE is used as a substitute for capacitor in Fig. 3, to fit more accurately the impedance behavior of the electric double-layer. Constant phase elements CPE have widely been used to account for deviations brought about by surface roughness.

4.1.3. Potentiodynamic polarization measurements

Figure 5 shows typical polarization curves for the inhibition characteristics of TME.

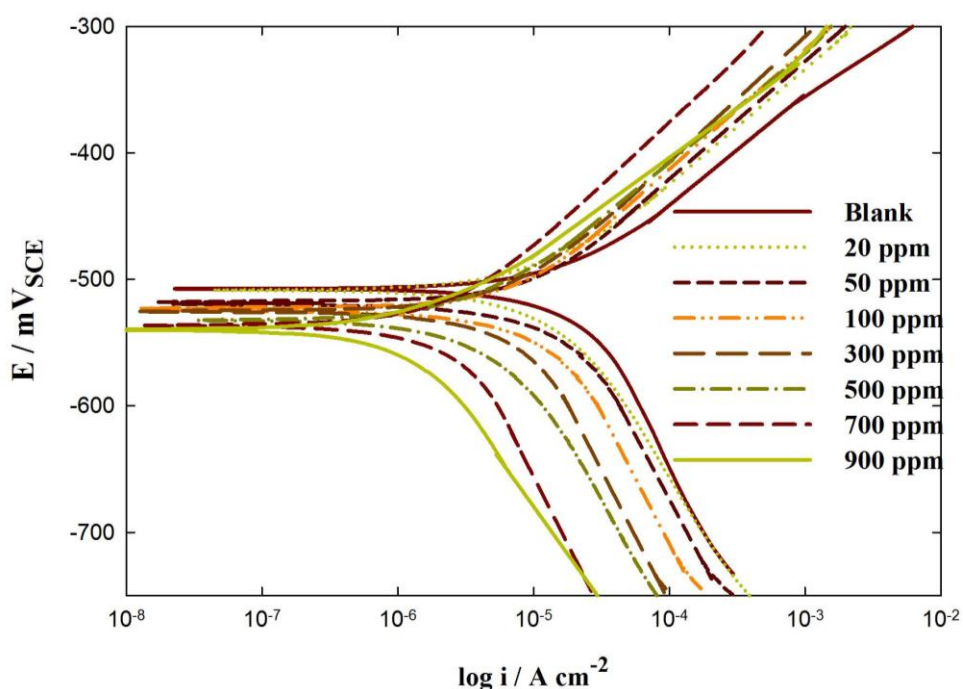


Figure 5. Polarization curves for iron in 1.0 M HCl in the absence and presence of various concentrations of TME at 30 °C ± 1

Curves in Fig. 5 show that the anodic and cathodic polarization curves recorded on iron electrode in 1.0M HCl at various concentrations in the presence and absence of TME. As would be expected both anodic and cathodic reactions of iron electrode corrosion were inhibited with the increase of TME concentration. This result suggests that the addition of TME reduces anodic dissolution and also retards the hydrogen evolution reaction.

Table 3. Electrochemical kinetic parameters, protection efficiencies (E_p %) and rates of corrosion associated with Tafel polarization measurements recorded for in 1.0 M HCl solutions without and with various concentrations of TME at 30 °C \pm 1.

[Inhib]	$\beta_a /$ mV dec ⁻¹	$\beta_c /$ mV dec ⁻¹	-E _{corr} / mV(SCE)	$(i_{corr}) /$ $\mu\text{A cm}^{-2}$	C.R. mpy	E_p %
Blank	85.02	198.7	507.5	20.07		---
20 ppm	95.7	166.0	508.5	12.97	5.927	35.37
50 ppm	98.6	164.4	518.6	11.37	5.197	43.34
100 ppm	101.6	170.9	523.6	9.0	4.114	55.15
300 ppm	104	178.9	525.2	7.783	3.557	61.22
500 ppm	91.33	170.1	532.1	4.486	2.051	77.64
700 ppm	105.7	191.3	536.2	3.043	1.391	84.84
900 ppm	98.94	187.4	540.3	1.524	0.696	92.41

Table 3 shows the electrochemical corrosion kinetic parameters, i.e. corrosion potential (E_{corr}), cathodic and anodic Tafel slopes (β_c , β_a) and corrosion current density i_{corr} obtained by extrapolation of the Tafel lines. The calculated inhibition efficiency, E_p (%) are also reported from equation (15),

$$E_p \% = \left(1 - \frac{i_{\text{corr}}}{i_{\text{corr}}^o}\right) \times 100 \quad (15)$$

where i_{corr}^o and i_{corr} are uninhibited and inhibited corrosion current densities, respectively. It can be seen that by increasing inhibitor concentration, the corrosion rate decreased and inhibition efficiency E_p %, increased. A cathodic shift was observed in the E_{corr} values, in the presence of various concentrations of TME, suggesting that TME behaves as cathodic-type inhibitor. Moreover, this inhibitor causes no significant change in the anodic and cathodic Tafel slopes, indicating that the inhibitor is first adsorbed onto iron surface and therefore impedes by merely blocking the reaction sites of iron surface without affecting the anodic and cathodic reaction mechanism.

4.2 Computational study

4.2.1 Local reactivity of the TME

Frontier molecular orbital theory helps in predicting adsorption centers of the inhibitor molecules responsible for the interaction with surface metal atoms [4,29]. Frontier molecular orbitals could provide dominative contribution, because of the inverse dependence of stabilization energy on orbital energy difference [29]. Table 4 presents the calculated energy levels of the HOMO and LUMO orbitals for the studied TME molecule. Moreover, the energy gap between the LUMO and HOMO energy levels of the molecules which is another important factor that should be considered is also

calculated. It is reported that excellent corrosion inhibitors are those organic compounds who not only give electrons to unoccupied orbital of the metal, but also accept free electrons from the metal [30].

Table 4. Quantum chemical descriptors for TME using DFT calculations

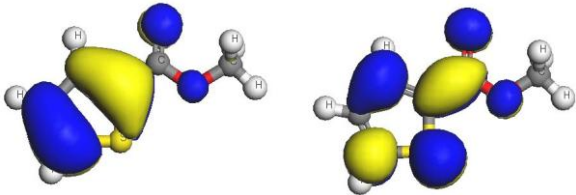
HOMO (eV)	LUMO (eV)	Energy gap (LUMO-HOMO), eV	Surface Area (\AA^2)	Dipole Moment (e \AA)	Molecular Volume (\AA^3)
-9.298	-1.3407	7.9573	166.886	3.135	128.453
					

Table 4 shows the highest occupied molecular orbital (HOMO) and the lowest unoccupied molecular orbital (LUMO) of the molecules under study. From this Table, it can be observed that the investigated thiophene derivative present a clear contribution of π -orbitals pertaining to the thiophene rings on the HOMO and LUMO.

In Table 4, a representation of the HOMO and LUMO orbitals calculated in the presence of a solvent (water). As can be seen from Table 4 that, HOMO is located in the thiophene ring as well as the side chains attached to this moiety. This would indicate that the preferred active sites for an electrophilic attack are located within the region around the sulphur atom belonging to the thiophene ring.

The quantum chemical calculations depicted in Table 4 revealed that TME has relatively high HOMO, low energy gap and low dipole moment which is explain its high inhibition efficiency from theoretical point of view. The higher the HOMO energy of the inhibitor, the greater the trend of offering electrons to unoccupied d orbital of the iron metal, and the higher the corrosion inhibition efficiency for iron in HCl acid solutions; in addition, the lower the LUMO energy, the easier the acceptance of electrons from metal surface, as the LUMO–HOMO energy gap decreased and the efficiency of inhibitor improved [31].

Fukui functions rationalize the reactivity of individual molecular orbital contributions to account for the response of the whole molecular spectrum and not only of the frontier orbitals. Mineva et al. [32] presented several benchmark applications of this protocol describing selectivity and reactivity by means of orbital Fukui indices. The reactivity indices are not directly attained experimentally and only the relative trends between theoretical data and experimental information can be compared and analyzed. With the aim of having a wider knowledge about the local reactivity of TME, the Fukui indices for TME has been calculated and analyzed along with the distribution of charges and provides a more complete scheme of the reactivity of TME [33]. The calculated Fukui indices for all the charged species ($N + 1$ and $N - 1$) as well as the neutrals (N) of each of the studied inhibitors are presented in Table 4. For simplicity, only the charges and Fukui functions over the

oxygen (O), sulphur (S) and carbon atoms are presented [31]. The optimized structures for TME in its ground states are shown in Fig. 1.

The site for nucleophilic attack will be the place where the value of f_k^+ is a maximum. In turn, the site for electrophilic attack is controlled by the value of f_k^- . The values of the Fukui functions for a nucleophilic and electrophilic attack are given for the investigated compounds in Table 5, only for the oxygen atom, sulphur atom and carbon atoms. Inspection of Table 5 shows that the electrophilic character, f_k^- of TME is concentrated around the sulphur atom S(5) as well as O(7) and O(8). Based on Fukui indices in Table 5, it can be concluded that the TME compound has more electrophilic power, f_k^- as it is indicated in Table 5 will have many active centers for adsorption on iron surface. These areas of S and O atoms are the most possible sites of bonding iron surface by donating electrons to the iron surface as indicated from Table 5.

Table 5. Calculated Mulliken atomic charges and Fukui functions for TME using DFT calculations.

Inhibitor	Atom	$q_k(N)$	$q_k(N+1)$	$q_k(N-1)$	f_k^+	f_k^-	f_k^0
2-thiophenecarboxylic acid methyl ester	C(1)	0.105	0.125	0.015	0.020	0.09	0.055
	C(2)	-0.231	-0.153	-0.277	0.078	0.046	0.046
	C(3)	-0.166	-0.150	-0.220	0.016	0.054	0.035
	C(4)	-0.159	-0.079	-0.258	0.080	0.099	0.050
	S(5)	-0.135	0.066	-0.406	0.201	0.271	0.186
	C(6)	0.454	0.552	0.420	0.098	0.034	0.066
	O(7)	-0.419	-0.30	-0.519	0.119	0.10	0.109
	O(8)	-0.414	-0.383	-0.539	0.031	0.125	0.028
	C(9)	-0.406	-0.439	-0.378	-0.033	-0.028	0.030

In this study, instead of calculating the molecular orbitals for the neutral, cation, and anion, we can add or subtract an electron from the molecular orbitals of the neutral molecule. This procedure gives a quick graphical display of the susceptibility of different kinds of attack.

4.2.2 Molecular dynamics simulation

Adsorption of TME molecules has been studied using molecular dynamics simulation techniques. Adsorption of TME on iron substrate, Fe (110) has been studied to find the lowest energy adsorption sites on TME molecules. Adsorption energy of TME on iron substrate has been presented in Fig. 6. Figure 6 shows the adsorption energy distribution of TME on iron substrate. The most stable configuration for adsorption of TME molecules on iron substrate is presented in Fig. 7. As can be seen from Fig. 7 that sulphur and oxygen atoms play the main role of adsorption of TME on Fe (110) substrate. The outputs and descriptors calculated by the Monte Carlo simulation method are presented in Table 6.

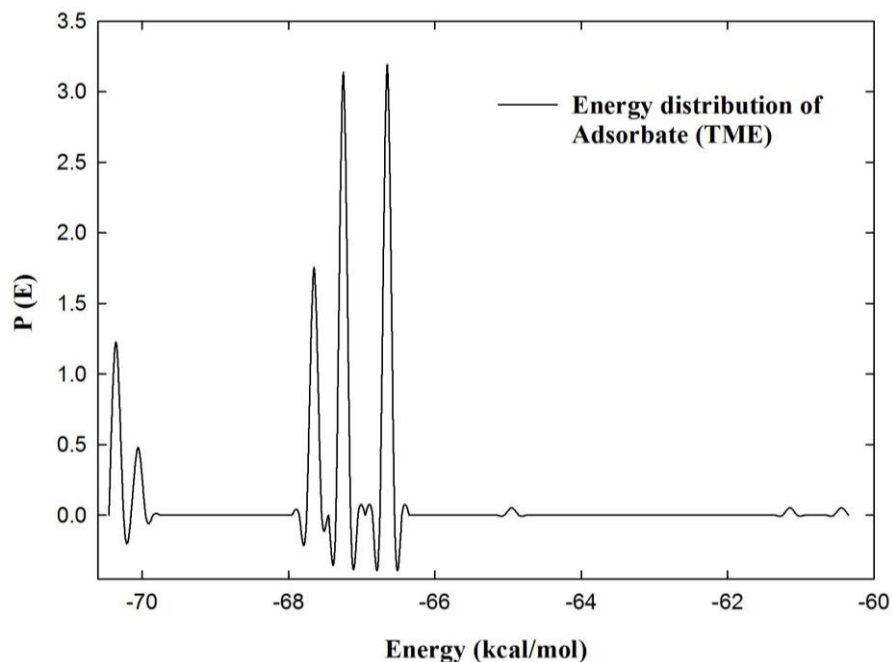


Figure 6. The adsorption energy distribution of the adsorbate TME on Fe (110)

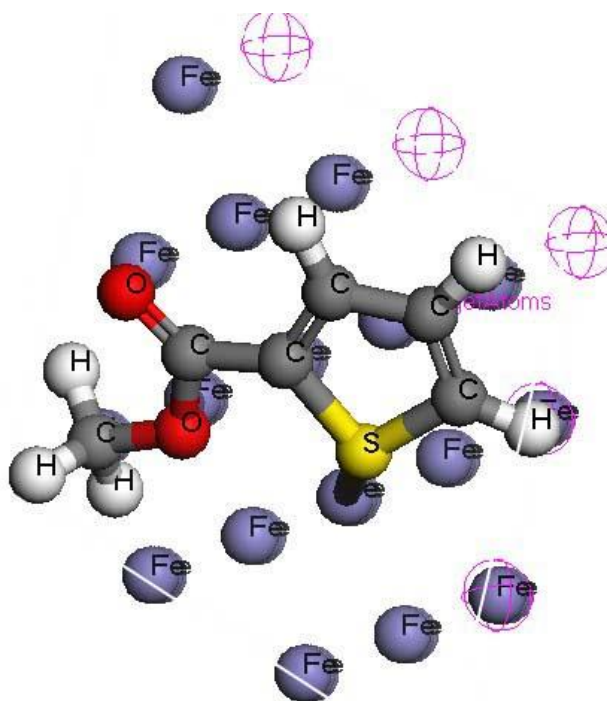


Figure 7. The most stable configuration for adsorption of TME molecules on iron substrate (110)

The parameters presented in Table 6 include total energy, in kcal mol^{-1} , of the substrate-adsorbate configuration. The total energy is defined as the sum of the energies of the adsorbate components, the rigid adsorption energy and the deformation energy. In this work, the substrate energy (iron surface) is taken as zero. In addition, adsorption energy in kcal mol^{-1} , reports energy released (or

required) when the relaxed TME molecules are adsorbed on the Fe(110). The adsorption energy is defined as the sum of the rigid adsorption energy and the deformation energy for the TME molecules.

Table 6. Outputs and descriptors calculated by the Mont Carlo simulation for adsorption of TME on iron (110)

Inhibitor	Total energy kcal mol ⁻¹	Adsorption energy/ kcal mol ⁻¹	Rigid adsorption / energy kcal mol ⁻¹	Deformation energy/ kcal mol ⁻¹	dE _{ad} /dN _i kcal mol ⁻¹	Calculated binding energy / kcal mol ⁻¹
TME	-25.69	-70.33	-74.4	4.07	-70.33	235.5

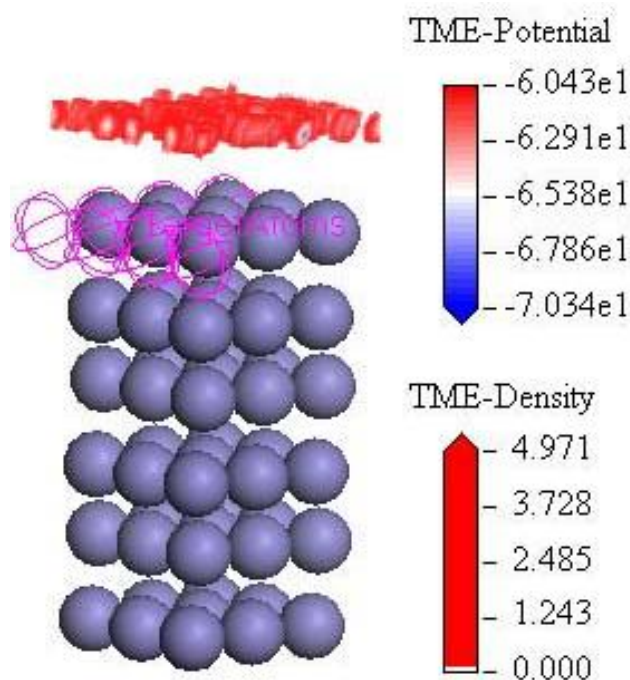


Figure 8. The adsorption density field of TME molecules on the Fe (110) substrate

The rigid adsorption energy reports the energy, in kcal mol⁻¹, released (or required) when the unrelaxed TME molecules, before the geometry optimization step) are adsorbed on the Fe (110). The deformation energy reports the energy, in kcal mol⁻¹, released when the adsorbed TME molecules are relaxed on the substrate surface. Table 6 shows also (dE_{ads}/dN_i), which reports the energy, in kcal mol⁻¹, of Fe-TME configurations where one of the TME molecules has been removed. The binding energy between TME molecules and iron substrate is introduced in Table 6 calculated from Eq. (7). As can be seen from Table 6, TME molecules give high adsorption energy during the simulation process. High values of adsorption energy indicate that TME molecules are possible efficient inhibitor. The adsorption density of TME on the Fe (110) substrate has been presented in Fig. 8. Therefore, the studied molecules are likely to adsorb on the iron surface to form stable adsorption layers and protect iron from corrosion.

4.3 Mechanism of adsorption of TME molecules

Adsorption of 2-thiophenecarboxylic acid methyl ester TME can be described by two main types of interactions: physical adsorption and chemisorption. Generally, physical adsorption requires the presence of both the charged metal surface and charged ions in solution. Chemisorption process involves charge sharing or charge-transfer from the inhibitor molecules to the metal surface to form a coordinate type of a bond. This is possible in the case of a positive as well as a negative charge of the surface [33].

The presence of a transition metal such as iron, having vacant d orbital, low-energy electron orbitals and of an inhibitor with molecules having relatively loosely bound electrons or hetero-atoms with a lone pair of electrons is necessary [34].

In aqueous acidic solutions, TME molecules exist either as neutral molecules or in the form of cations. TME molecules may be adsorbed on the metal surface in the form of neutral molecules involving the displacement of water molecules from the metal surface and sharing of electrons between the sulphur atom and the iron surface (chemical adsorption).

The high inhibition efficiency of TME is due to the presence of other probable sites susceptible to electrophilic attack, namely S(5), O(7) and O(8) as well as low HOMO energy, low energy gap and low dipole moment.

5. CONCLUSION

The following results can be drawn from this study:

1. Experimental investigations of the studied thiophene derivative show that it reduces the corrosion rate of iron remarkably as its concentration increases.
2. Polarization studies show that TME molecules act as cathodic-type inhibitor.
3. The presence of sulphur and oxygen atoms as well as π -electrons enables the interaction and bonding between TME and iron surface.
4. The quantum mechanical approach as well as molecular dynamics simulation techniques may well be able to foretell molecule structures that are better for corrosion inhibition.

ACKNOWLEDGMENT

The authors acknowledge the financial of the work project 1-432-1128 provided by Taif University.

References

1. H. Ashassi-Sorkhabi, N. Ghalebsaz-Jeddi, *Mat. Chem. and Phys.*, 92 (2005) 480.
2. G. Trabanelli, *Corrosion* 47 (1991) 410.
3. M. Ajmal, A.S. Mideen, M.A. Quaraishi, *Corros. Sci.*, 36 (1994) 79.
4. J. Fang, J. Li, *J. Mol. Str. (Theochem)* 593 (2002) 179–185
5. B. Donnelly, T.C. Downie, R. Grzekowiak, H.R. Hamburg, D. Short, *Corros. Sci.*, 18 (1978)109.
6. H. Brandt, M. Fischer, K. Schawabe, *Corros. Sci.*, 10 (1970) 631.

7. A.Chetouani, A. Aouniti, B. Hammouti, N. Benchat, T. Benhadda, S. Kertit, *Corros. Sci.*, 45 (2003) 1679.
8. M. Bouklah, B. Hammouti, T. Benhadda, M. Benkaddour, *J. Appl. Electrochem.*, 35 (2005)1095.
9. A.Ouchrif, A. Yahyi, B. Hammouti, A. Dafali, M. Benkaddour, A. Et-Touhami, *Bull. Electrochem.*, 19 (2003) 455.
10. S. Elayyoubi, E.B. Maarouf, H. Oudda and B. Hammouti, *Bull. Electrochem.*, 18 (2002) 45.
11. S.S. Abdel-Rehim, K.F.Khaled and N.S. Abdel-Shafi, *Electrochim. Acta*, 51 (2006) 3267.
12. R.W. Bosch, J. Hubrecht, W.F. Bogaerts and B.C. Syrett, *Corrosion* 57 (2001) 60.
13. R.W. Bosch and W.F. Bogaerts, *Corrosion* 52 (1996) 204.
14. K.F. Khaled, *Appl. Surf. Sci.*, 255 (2008) 1811-1818.
15. K.F. Khaled, *Appl. Surf. Sci.*, 256 (2010) 6753-6763.
16. K.F. Khaled, S.S. Abdel-Rehim, N. Hackerman, *Ann. Univ. Ferrara* 2 (2000) 713.
17. W. Yang, W. J. Mortier, *J. Am. Chem. Soc.*, 108 (1986) 5708.
18. F. Méndez , M. Galván, A. Garritz, A. Vela, J. Gázquez, *J. Mol. Str.*, 277 (1992) 1981.
19. K.F. Khaled, *J. Solid State Electrochem.*, 13 (2009) 1743.
20. K.F.Khaled , Sahar A. Fadl-Allah and B. Hammouti *Mater. Chem and Phys.*, 117 (2009) 148.
21. B. Delley , *J. Chem. Phys.*, 92 (1990) 508.
22. B. Delley , *J. Chem. Phys.*, 113 (2000) 7756.
23. R. S. Mulliken, *J. Chem. Phys.*, 23 (1995) 1833.
24. K.F.Khaled, *J. Appl. Electrochem.*, 39 (2009) 429-438.
25. K. Hladky, L. M. Callow, J. L. Dawson, *Br. Corros. J.*, 15 (1980) 20.
26. R. L. Hurt , J. R. Macdonald, *Solid State Ionics* 111 (1986) 20.
27. L. Nyikos , T. Pajkossy, *Electrochim. Acta*, 30(1985) 1533.
28. J. R. Macdonald , *J. Electroanal. Chem.*, 223 (1987), 25-50
29. G. Bereket, E. Hür and C. Öğretir, *J. Mol. Struct. (Theochem)*, 578 (2002) 79.
30. P. Zhao, Q. Liang and Y. Li, *Appl. Surf. Sci.*, 252 (2005) 1596.
31. K.F.Khaled, *Corros. Sci.*, 2011, doi:10.1016/j.corsci.2011.01.035 in press
32. T. Mineva, V. Parvanov, I. Petrov, N. Neshev and N. Russo, *J. Phys. Chem. A*, 105 (2001) 1959.
33. J. Cruz, L.M. Martínez-Aguilera, R. Salcedo and M. Castro, *Int. J. Quant. Chem.* 85 (2001) 546.
34. K. F. Khaled and M. Amn, *Corros. Sci.*, 51 (2009) 2098–2106
35. J.G.N. Thomas, in: Proc. 5th Europ. Symp. on Corrosion Inhibitors, Ann. Univ. Ferrara, Italy, 1980, 1981, pp. 453.